

A new approximation method for scattering by long finite arrays

I Thompson*, C M Linton* and R Porter†

*Dept. of Mathematical Sciences, Loughborough University, Leicestershire, LE11 3TU, UK

† Dept. of Mathematics, University of Bristol, Bristol, BS8 1TW, UK

Abstract

The scattering of water waves by a long array of rigid vertical circular cylinders is analysed under the usual assumptions of linear theory. Our primary goal is to show how solutions obtained for semi-infinite arrays can be combined to provide accurate and numerically efficient solutions to problems involving long, but finite, arrays. The particular diffraction problem considered here has been chosen both for its theoretical interest and its applicability. The design of offshore structures supported by cylindrical columns is commonplace and understanding how the multiple interactions between the waves and the supports affect the field is clearly important. The theoretical interest comes from the fact that, for wavelengths greater than twice the geometric periodicity, the associated infinite array can support Rayleigh–Bloch surface waves that propagate along the array without attenuation. For a long finite array we expect to see these surface waves travelling back and forth along the array and interacting with the ends. For particular sets of parameters, near trapping has previously been observed and we provide, for the first time, a quantitative explanation of this phenomenon based on the excitation and reflection of surface waves by the ends of the finite array.

1 Introduction

Phenomena associated with scattering by large finite arrays are of practical importance in many physical contexts. Examples include the design of photonic and phononic band-gap materials, the performance of phased-array antennas, and the hydrodynamic characteristics of structures supported on an array of columns. The relevant scattering problems can often be solved directly, but the computational cost increases rapidly as the number of elements in the array increases.

In some cases it may be appropriate to model the large finite array as an infinite array so that the resulting geometrical periodicity can be used to greatly simplify the necessary analysis. One might expect that this would lead to solutions that are valid in the interior of the array, far from any ends or edges. Thus, for example, the claim is made in [1] (in the context of electromagnetic scattering) that “finite periodic structures behave like their infinite counterparts”. However, in this article we are concerned with a situation where this is manifestly not the case due to the excitation of surface waves that propagate along the array without decay. Array guided surface waves have been observed numerically in arrays of dipoles [2], and microstrip antennas are designed so as to suppress surface wave production [3], but theoretical techniques for studying the excitation of such waves by array edges are few and far between. Recently [4], accurate techniques for the determination of the amplitude of surface waves excited by the end of a semi-infinite array have been developed and this article builds on that work.

The particular problem that we consider is that of water-wave scattering by an array of vertical circular cylinders which, once the depth dependence has been factored out, is equivalent to two-dimensional acoustic scattering by a one-dimensional finite array of circles. The

direct computation of the solution is fairly straightforward in this example but, as we shall demonstrate, the approximation described below significantly reduces execution time when large numbers of scatterers are involved. Moreover, we are able to shed considerable light on the phenomenon of near-trapping, first reported for this type of array in [5]. The frequencies at which surface waves (known as Rayleigh–Bloch waves in this context) propagate along an infinite periodic array of such structures were computed in [6, 7]; these are a generic phenomenon associated with rigid periodic structures [8, 9].

The idea behind our approximation method is simple. We assume the array is sufficiently long that any fields generated at one end which decay along the array do not interact with the other end. Surface waves that are excited do not decay and so their interactions with the other end of the array are included. We thus construct the solution to the finite array problem from those to a number of canonical problems, all formulated on infinite or semi-infinite arrays. Of course, for this approach to be of use, it is vital that the solutions to these canonical problems can be computed accurately and efficiently.

An example of some of the interesting effects that we seek to explain is shown in Figure 1. Here the scattering of a plane wave by a 101-cylinder array is considered, the incident field being aligned with the array (head-on incidence). All lengths are scaled so that the distance between the centres of consecutive elements is unity; according to this scaling, the radius of the circles is 0.25. The two graphs show the magnitude of the horizontal forces (i.e. the integral of the pressure times the component of the normal to the cylinders along the array) acting on cylinders 0 (\mathcal{F}_x^0) and 50 (\mathcal{F}_x^{50}) compared with those computed for a semi-infinite array, plotted against the wavenumber k ($= 2\pi/\lambda$). The forces are normalised so that they would be unity for a scatterer in isolation. Since there is no excitation of the right end by the incident field, one might naively expect the results to be similar, and this is indeed the case for small k , and also for $k \gtrsim 2.8$. However, as k increases toward 2.8, an oscillation builds up in the forces on the finite array, and the semi-infinite array solution fails to capture this effect. In particular, there is a value of k close to 2.8 about which the oscillations become so large that the force on scatterer 50 is around 35 times that on an isolated scatterer.

The structure of the paper is as follows. The problem is formulated in §2 and then reduced to a series of canonical problems. The accuracy of the approach is discussed in §3 and then in §4 we show how the excitation of surface waves by the array ends can lead to constructive interference and a near-trapping phenomenon.

2 Formulation

We consider the scattering of time-harmonic water waves by vertical circular cylinders in water of constant depth under the usual assumptions of linear theory. The motion is governed by a velocity potential Φ which satisfies the three-dimensional Laplace equation but this can be reduced to a two-dimensional boundary-value problem by writing

$$\Phi(x, y, z) = \text{Re}[\phi(x, y) \cosh k(z + h)e^{-i\omega t}]. \quad (1)$$

Here, h is the quiescent water depth, and ω is the angular frequency. The function ϕ satisfies the two-dimensional Helmholtz equation $(\nabla^2 + k^2)\phi = 0$ in the region exterior to the scatterers, and these are now circles in the (x, y) -plane. The wavenumber k is the positive solution to the dispersion relation $k \tanh kh = \omega^2/g$, where g is the acceleration due to gravity. With a different definition of k exactly the same problem governs the scattering

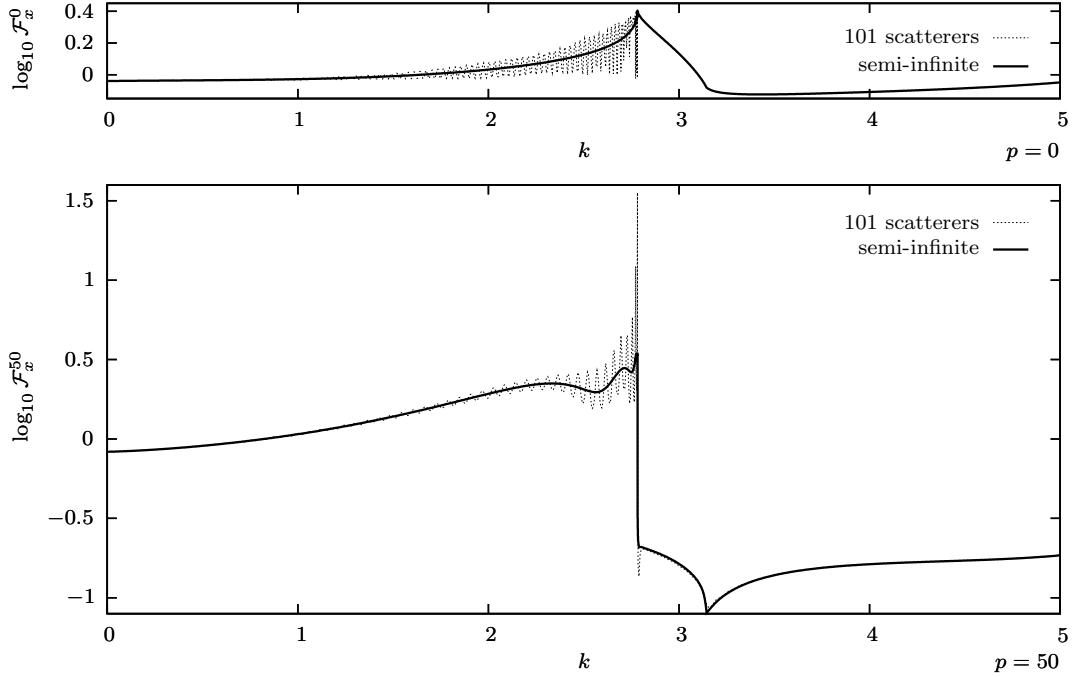


Figure 1: Horizontal force exerted on scatterer p ($p = 0$ upper, $p = 50$ lower) at head-on incidence for a 101-cylinder array plotted against wavenumber.

of acoustic waves by an array of circles. The scatterers are assumed to be rigid so that the appropriate boundary condition on their surface is $\partial\phi/\partial n = 0$, where ∂n is an element of the outgoing normal.

The subject of our investigation is the scattering of a plane wave

$$\phi_{\text{inc}} = e^{ik(x \cos \psi_0 + y \sin \psi_0)}, \quad (2)$$

by a long linear array of circular scatterers, each of which has radius a . All lengths in the problem are scaled so that the centre of scatterer p is located at the point $(p, 0)$, where $p \in \{0, 1, \dots, P\}$; see figure 2. We treat this problem by assuming that P is sufficiently large so that the ends $x = 0$ and $x = P$ can be treated independently, except in situations where Rayleigh–Bloch surface waves are excited. Such waves are excited at low-frequencies by the end of a semi-infinite array and methods for accurately determining their amplitude have been developed in [4].

To construct the solution, we must consider several canonical array problems. For brevity, we introduce the term ‘ $\{p_0, p_1\}$ array’ to refer to the array that consists of scatterers centred at $(p, 0)$ where $p \in \{p_0, \dots, p_1\}$. The solution to such a problem can be written in the form $\phi = \phi_{\text{inc}} + \phi_{\text{sc}}$, where

$$\phi_{\text{sc}} = \sum_{p=p_0}^{p_1} \sum_{m=-\infty}^{\infty} \mathcal{U}_m^p Z_m H_m(kr_p) e^{im\theta_p}. \quad (3)$$

Here, $H_m \equiv H_m^{(1)}$ is a Hankel function of the first kind, (r_p, θ_p) is a set of polar co-ordinates with its origin at the centre of scatterer p , and the factors $Z_m = J'_m(ka)/H'_m(ka)$ have been

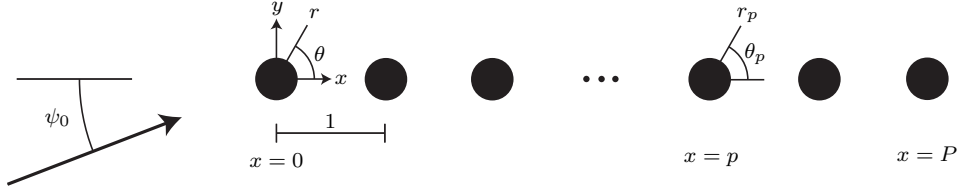


Figure 2: Schematic diagram showing a plan view of the finite array.

introduced for convenience. The coefficients \mathcal{U}_n^p satisfy the linear system [10]

$$\mathcal{U}_m^p + \sum_{n=-\infty}^{\infty} Z_n \sum_{\substack{j=p_0 \\ \neq p}}^{p_1} \mathcal{U}_n^j X_{n-m}^{p-j} \mathbf{H}_{n-m}(k|j-p|) = \mathcal{R}_m^p \quad p = p_0, \dots, p_1, \quad m \in \mathbb{Z}, \quad (4)$$

in which $X_n^j = (\text{sgn } j)^n$. The quantity \mathcal{R}_m^p appearing on the right-hand side is determined by the expansion of the incident field about the centre of the p th cylinder, i.e.

$$\phi_{\text{inc}} = \sum_{m=-\infty}^{\infty} \mathcal{R}_m^p Z_m \mathbf{J}_m(kr_p) e^{im\theta_p}. \quad (5)$$

For a plane wave incident at angle ψ_0 we have

$$\mathcal{R}_m^p = -e^{ipk \cos \psi_0} \mathbf{i}^m e^{-im\psi_0}. \quad (6)$$

2.1 The infinite array

We will make explicit the dependence of the unknown coefficients on the angle of incidence; thus for the $\{-\infty, \infty\}$ array, we have

$$\mathcal{U}_m^p = B_m(\psi_0) e^{ipk \cos \psi_0}, \quad (7)$$

and the coefficients $B_m(\psi_0)$ are easily obtained, see [11], [12]. Due to the symmetry of the array about $x = 0$, we have

$$B_{-m}(\pi - \psi_0) = B_m(\psi_0). \quad (8)$$

We will refer to (7) as the solution to the $\{-\infty, \infty\}$ problem. This solution is said to be right (left) resonant if there exists $j \in \mathbb{Z}$ such that $\psi_j = 0$ ($\psi_j = \pi$), where

$$\cos \psi_j = \cos \psi_0 + 2j\pi/k, \quad j \in \mathbb{Z}. \quad (9)$$

The finite set of real values for ψ_j corresponds to the angles at which plane waves are scattered by the array. Resonance implies that one of these scattered waves propagates exactly parallel to the array. This is an important special case which has some bearing on the accuracy of our method. Note that, if $\psi_0 = 0$ (or π), then $B_m = 0$ for all m ; in this case the scattered field simply cancels the incident wave [12].

The $\{-\infty, \infty\}$ array can also support periodic homogeneous solutions known as Rayleigh–Bloch waves. Thus, if we take $\mathcal{R}_m^p = 0$ and write

$$\mathcal{U}_m^p = \tilde{B}_m e^{ip\tilde{\beta}}, \quad (10)$$

then (4) reduces to

$$\tilde{B}_m + \sum_{n=-\infty}^{\infty} \tilde{B}_n Z_n \sigma_{n-m}(\tilde{\beta}) = 0, \quad m \in \mathbb{Z}, \quad (11)$$

where σ_n is the Schlömilch series of order n , i.e.

$$\sigma_n(\lambda) = \sum_{j=1}^{\infty} [(-1)^n e^{i\lambda j} + e^{-i\lambda j}] H_n(kj). \quad (12)$$

These series can be evaluated efficiently using formulae in [13] and [14]. The values of $\tilde{\beta}$ for which (11) possesses a nontrivial solution can easily be determined (the system can in fact be reduced to one with real coefficients), as can the nontrivial solution itself; see [7]. This is normalised so that

$$\sum_{m=-\infty}^{\infty} |\tilde{B}_m Z_m|^2 = 1. \quad (13)$$

Equations (11) and (13) define the coefficients \tilde{B}_m up to a common phase factor, which is unimportant provided that the same value is used consistently. Computations show that for a given frequency and scatterer radius, up to two values of $\tilde{\beta}$ can exist in the interval $(0, \pi)$. One of these corresponds to a Rayleigh–Bloch wave that is symmetric about $y = 0$, the other to an antisymmetric mode. Both of these modes propagate (i.e. transport energy) in the direction of increasing x and are represented by a potential of the form

$$\phi_{\text{rb}}(\tilde{\beta}) = \sum_{p=-\infty}^{\infty} \sum_{m=-\infty}^{\infty} \tilde{B}_m e^{ip\tilde{\beta}} Z_m H_m(kr_p) e^{im\theta_p}. \quad (14)$$

It follows from (12) that $\sigma_n(-\lambda) = (-1)^n \sigma_n(\lambda)$ and hence if there is a solution to (11) for $\tilde{\beta} > 0$, then there is a solution for $-\tilde{\beta}$ with $\tilde{B}_m(-\tilde{\beta}) = (-1)^m \tilde{B}_m(\tilde{\beta})$. These represent equivalent left-propagating modes which we will choose to write as

$$\phi_{\text{rb}}(-\tilde{\beta}) = \pm \sum_{p=-\infty}^{\infty} \sum_{m=-\infty}^{\infty} (-1)^m \tilde{B}_m e^{-ip\tilde{\beta}} Z_m H_m(kr_p) e^{im\theta_p}. \quad (15)$$

Here, the upper and lower signs refer to the symmetric (about $y = 0$) and antisymmetric cases, respectively. This sign convention is purely for later algebraic convenience and will be used throughout. Note that \tilde{B}_m will always be used to refer to the solution to (11) for $\tilde{\beta} \in (0, \pi)$. Due to the periodicity in (10), there are no distinct solutions for other real values of $\tilde{\beta}$.

The mode which is symmetric about $y = 0$ exists for all scatterer sizes, but the antisymmetric mode only exists for $0.403 \lesssim a \leq 0.5$. For a given value of a , Rayleigh–Bloch waves exist for a range of values of k ; symmetric modes in the range $0 < k < k_{\text{max}}^s < \pi$ and antisymmetric modes in the range $k_{\text{min}}^a < k < k_{\text{max}}^a < \pi$. It turns out that there are three distinct regimes: for $a \lesssim 0.403$ only symmetric modes are possible; for $0.403 \lesssim a \lesssim 0.459$ we have $k_{\text{max}}^s < k_{\text{min}}^a$ and so it is possible to have symmetric and antisymmetric modes, but not for the same value of k ; finally when $0.459 \lesssim a < 0.5$ we have $k_{\text{max}}^s > k_{\text{min}}^a$ and hence it is only in this parameter range that it is possible to excite both symmetric and antisymmetric modes at the same time. Curves showing how k_{max}^s , k_{min}^a and k_{max}^a vary with scatterer radius a can be found in [4].

Henceforth, we shall assume that only one Rayleigh–Bloch wave is present, cases in which both modes are excited can be treated by separating the vertically symmetric and antisymmetric parts of the problem and solving these individually. For any array solution that has been decomposed in this way, we have

$$\mathcal{U}_m^p = \pm(-1)^m \mathcal{U}_{-m}^p. \quad (16)$$

2.2 Semi-infinite arrays

Methods for computing the solution for the $\{0, \infty\}$ array have been developed in [4]. In this case we write $\mathcal{U}_m^p = A_m^p(\psi_0)$, where $A_m^p(\psi_0)$ is composed from a sum of three terms; thus

$$A_m^p(\psi_0) = e^{ipk \cos \psi_0} B_m(\psi_0) + \alpha(\psi_0) e^{ip\tilde{\beta}} \tilde{B}_m + C_m^p(\psi_0). \quad (17)$$

The first contribution on the right hand side is the equivalent coefficient for the $\{-\infty, \infty\}$ array, and the second is due to a right propagating Rayleigh–Bloch wave. If we were to make a different choice for the coefficients \tilde{B}_m (recall that these are defined up to a multiplicative phase factor by (11) and (13)), then the value of α would also change, so that the product $\alpha \tilde{B}_m$ remains the same. The final term, $C_m^p(\psi_0)$, decays as $p \rightarrow \infty$; its contribution to the field is a circular wave radiating from the end. Note that decomposing the coefficients in this way is not the same as decomposing the potentials, since the solutions to problems for different arrays exist on different fluid domains. The leading order behaviour of the coefficients C_m^p as $p \rightarrow \infty$ is given by

$$C_m^p(\psi_0) \sim C_m(\psi_0) e^{ikp} p^{-u}, \quad (18)$$

with $u = 3/2$ in all cases except that of right resonance, when $u = 1/2$ [4]. This increase in the significance of the decaying end effects is the most important consequence of resonance in the context of the large array approximation. Head-on incidence ($\psi_0 = 0$) always leads to right resonance, regardless of the value of k (see equation(9) and subsequent discussion).

We also require the solution for the $\{-\infty, P\}$ array under plane-wave excitation. Here we write $\mathcal{U}_m^p = \hat{A}_m^p$, and these coefficients can be obtained in terms of A_m^p as follows. In (4) we can take $p_0 = 0$, let $p_1 \rightarrow \infty$ and replace j and P with $P - j$ and $P - p$, respectively. Note that $X_n^{(P-j)-(P-p)} = (-1)^n X_n^{j-p}$ and so we also make the transformations $n \rightarrow -n$ and $m \rightarrow -m$. The left-hand side of (4) is now identical to that which occurs in the $\{0, \infty\}$ array problem, with $A_m^p(\psi_0)$ replaced by $\hat{A}_{-m}^{P-p}(\psi_0)$. From (6), we have

$$\mathcal{R}_{-m}^{P-p}(\psi_0) = -e^{i(P-p)k \cos \psi_0} (-i)^m e^{im\psi_0}. \quad (19)$$

It therefore follows that

$$\hat{A}_m^p(\psi_0) = e^{iPk \cos \psi_0} A_{-m}^{P-p}(\pi - \psi_0), \quad p = P, P - 1, \dots \quad (20)$$

Substituting this into (17) and then making use of (8) and (16) yields

$$\hat{A}_m^p(\psi_0) = e^{ipk \cos \psi_0} B_m(\psi_0) \pm \hat{\alpha}(\psi_0) e^{-ip\tilde{\beta}} (-1)^m \tilde{B}_m + \hat{C}_m^p(\psi_0), \quad (21)$$

where

$$\hat{\alpha}(\psi_0) = \alpha(\pi - \psi_0) e^{iP(k \cos \psi_0 + \tilde{\beta})} \quad \text{and} \quad \hat{C}_m^p(\psi_0) = e^{iPk \cos \psi_0} C_{-m}^{P-p}(\pi - \psi_0). \quad (22)$$

This is as we should expect; \hat{A}_m^p includes the same term involving B_m as does A_m^p , whereas the other contributions are determined from the $\{0, \infty\}$ solution with a plane wave incident at angle $\pi - \psi_0$ and appropriate phase shifts. From equation (9), we see that if the angle of incidence ψ_0 gives rise to a right resonance, then $\pi - \psi_0$ leads to a left resonance, and vice-versa. Left resonance affects the coefficients \hat{C}_m^p in the same way that right resonance affects C_m^p (see equation (18) and subsequent discussion). Where no ambiguity can occur, we will dispense with writing the dependence of the coefficients on ψ_0 .

Next we consider the $\{0, \infty\}$ array under excitation of a left propagating Rayleigh–Bloch wave incident from the far field, and in this case we set $\mathcal{U}_m^p = Q_m^p$. Since \mathcal{U}_m^p are the coefficients in the expansion of the scattered potential, each one will include a contribution from a right-propagating Rayleigh–Bloch wave, therefore we write

$$Q_m^p = \rho e^{ip\tilde{\beta}} \tilde{B}_m + T_m^p, \quad (23)$$

where $T_m^p \sim T_m e^{ikp} p^{-3/2}$ for some set of constants T_m as $p \rightarrow \infty$, and ρ is the end reflection coefficient. As before, the contribution from the terms that decay as p is increased represents a circular wave radiating from the end. The incident field for this problem can be taken, from (15), as

$$\phi_{\text{inc}} = \pm \sum_{p=0}^{\infty} \sum_{m=-\infty}^{\infty} (-1)^m \tilde{B}_m e^{-ip\tilde{\beta}} Z_m H_m(kr_p) e^{im\theta_p}. \quad (24)$$

Note that the sum over p could actually start at any non-negative integer, the difference between the incident fields is simply a finite sum of circular waves which would be absorbed in the coefficients T_m^p . Expanding (24) about the centre of cylinder p using Graf's addition theorem shows that

$$\mathcal{R}_m^p = \mp (-1)^m e^{-ip\tilde{\beta}} \tilde{B}_m \mp \sum_{n=-\infty}^{\infty} Z_n \sum_{\substack{j=0 \\ \neq p}}^{\infty} e^{-ij\tilde{\beta}} (-1)^n \tilde{B}_n X_{n-m}^{p-j} H_{n-m}(k|j-p|). \quad (25)$$

Since the Rayleigh–Bloch wave is a homogeneous solution to the $\{-\infty, \infty\}$ problem, this can be simplified to yield

$$\mathcal{R}_m^p = \pm e^{-ip\tilde{\beta}} \sum_{n=-\infty}^{\infty} (-1)^n Z_n \tilde{B}_n \sum_{j=1+p}^{\infty} e^{ij\tilde{\beta}} H_{n-m}(kj). \quad (26)$$

The slowly convergent sums over j can be calculated efficiently using expressions in [14] and then ρ and T_m^p can be calculated using the filtering methods developed in [4]. The cut-off frequency $k = k_{\text{max}}$ is a special case in which exact values can be deduced. Here, we have $\tilde{\beta} = \pi$, so that the Rayleigh–Bloch wave ceases to propagate and takes the form of a standing wave. Furthermore, $\sigma_{2m-1}(\pi) = 0$, and this causes the system of equations for \tilde{B}_m (11) to decouple into two components:

$$\tilde{B}_{2m} + \sum_{n=-\infty}^{\infty} Z_{2n} \tilde{B}_{2n} \sigma_{2(n-m)}(\pi) = 0, \quad (27)$$

$$\tilde{B}_{2m+1} + \sum_{n=-\infty}^{\infty} Z_{2n+1} \tilde{B}_{2n+1} \sigma_{2(n-m)}(\pi) = 0. \quad (28)$$

Numerical results have shown that, in the vertically symmetric case, (28) has a nontrivial solution, and $\tilde{B}_{2m} = 0$ for all m when $\tilde{\beta} = \pi$. The opposite is true in the antisymmetric case, i.e. (27) has a nontrivial solution, and $\tilde{B}_{2m+1} = 0$ for all m . For a system decoupled in this way we have, from (14) and (15),

$$\phi_{\text{rb}}(\pi) = -\phi_{\text{rb}}(-\pi). \quad (29)$$

Equation (4) with the right-hand side (25) can therefore be solved by taking $\rho = 1$ and $T_m^p = 0$; note that this is the trivial solution, i.e. the reflected mode exactly cancels the incident field. This cancellation is only possible when the Rayleigh–Bloch modes are standing waves (i.e. when $\tilde{\beta} = \pi$).

Finally, we consider excitation of the $\{-\infty, P\}$ array by a right-propagating Rayleigh–Bloch wave; in this case we denote the unknown coefficients \hat{Q}_m^p . The right-hand side can be determined as in the previous case, and after rewriting (4) so that p ranges from 0 to ∞ , we find that

$$\hat{Q}_m^p = e^{iP\tilde{\beta}} Q_{-m}^{P-p}. \quad (30)$$

Substituting this into (23) yields

$$\hat{Q}_m^p = \pm \hat{\rho} e^{-ip\tilde{\beta}} (-1)^m \tilde{B}_m + \hat{T}_m^p \quad (31)$$

with

$$\hat{\rho} = \rho e^{2iP\tilde{\beta}} \quad \text{and} \quad \hat{T}_m^p = e^{iP\tilde{\beta}} T_{-m}^{P-p}. \quad (32)$$

Again, this is as we should expect; the amplitude of the Rayleigh–Bloch wave is precisely that which occurs in the $\{0, \infty\}$ array, with an appropriate phase shift.

2.3 Long finite arrays

We now construct the solution for the $\{0, P\}$ array in the form (3) according to the large array approximation. Thus, we write $\mathcal{U}_m^p = F_m^p$, where

$$F_m^p = e^{ipk \cos \psi_0} B_m + \chi^{\text{R}} e^{ip\tilde{\beta}} \tilde{B}_m \pm \chi^{\text{L}} e^{-ip\tilde{\beta}} (-1)^m \tilde{B}_m + G_m^p + \hat{G}_m^p. \quad (33)$$

The coefficients are thus composed from the solution of the $\{-\infty, \infty\}$ problem, Rayleigh–Bloch waves travelling to the right and left with amplitudes χ^{R} and χ^{L} , respectively, and extra terms representing the local effects of the two ends (as usual the hatted coefficients refer to the end at $x = P$). The large array approximation is now obtained by assuming that the total amplitude of the right-propagating Rayleigh–Bloch wave is due to interactions of the incident plane wave and the left-propagating Rayleigh–Bloch mode with the left end. Similarly the left-propagating Rayleigh–Bloch mode comes from the interactions of the incident plane wave and the right-propagating Rayleigh–Bloch mode with the right end. This yields a pair of equations for χ^{L} and χ^{R} ; thus

$$\chi^{\text{R}} = \alpha + \rho \chi^{\text{L}}, \quad \chi^{\text{L}} = \hat{\alpha} + \hat{\rho} \chi^{\text{R}}, \quad (34)$$

and from these we obtain

$$\chi^{\text{R}} = \frac{\alpha + \rho \hat{\alpha}}{1 - \rho \hat{\rho}}, \quad \chi^{\text{L}} = \frac{\hat{\alpha} + \hat{\rho} \alpha}{1 - \rho \hat{\rho}}. \quad (35)$$

ka	< 0.001	< 0.35	< 0.5	< 0.8	< 1.5	< 2.0	> 2.0
N	2	3	5	8	10	12	15

Table 1: Order truncation N for numerical computations.

Likewise, for the circular waves that are excited, we have

$$G_m^p = C_m^p + \chi^L T_m^p, \quad \hat{G}_m^p = \hat{C}_m^p + \chi^R \hat{T}_m^p. \quad (36)$$

The finite array problem has thus been reduced to solving the infinite array problem and determining the appropriate Rayleigh–Bloch mode, then finding α and ρ using the methods from [4]. The quantities $\hat{\alpha}$ and $\hat{\rho}$ follow from (22) and (32), respectively. Finally, G_m^p and \hat{G}_m^p are determined from (36) and the unknowns F_m^p constructed via (33).

3 Accuracy & Performance

At the time of writing, exact results for semi-infinite arrays are not available, except in the case of isotropic point scatterers [15]. For the finitely large scatterers that are of interest here, we must use the filtering methods developed in [4]. These are approximate in that some decaying end effects are always discarded. The filtering methods yield approximate values for C_m^p (also T_m^p) for $p \leq P_c$, where P_c is a parameter known as the spatial truncation. Increasing P_c leads to improved accuracy at the cost of greater execution time. All gains in terms of performance are lost if P_c is chosen to be equal to the size of the long finite array, P . On the other hand, if $P_c < P$, then we must introduce a further approximation so as to obtain values for C_m^p when $P_c < p \leq P$. A simple means of achieving this is to assume that $C_m^{P_c}$ has reached its asymptotic limit so as to obtain approximate values for the coefficients C_m appearing in (18); thus

$$C_m = C_m^{P_c} e^{-ikP_c} P_c^u. \quad (37)$$

The coefficients T_m^p can be treated in exactly the same way. Clearly the use of (37) in those resonant cases where $u = 1/2$ will introduce greater errors than it does when $u = 3/2$, which is more usual. The sums over order must also be truncated, that is we must use a finite number of modes $-N \dots N$ to represent the field radiating from each individual scatterer. The truncation parameter N must be chosen to be large enough to yield accurate results, but not so large as to unnecessarily increase program execution time or generate near singular linear systems. The values used shown in table 1 have been found to satisfy these criteria.

If we define the percentage error on scatterer p via

$$E_p = 100 \times \frac{\sum_{n=-N}^N |Z_n(F_n^p - D_n^p)|}{\sum_{n=-N}^N |Z_n D_n^p|}, \quad (38)$$

where D_n^p is the coefficient that occurs when the $\{0, P\}$ array problem is solved directly, then this gives a stringent measure of the accuracy achieved by the large array approximation. Figure 3 shows logarithmic plots of E_p against p for a 101 scatterer array with various parameters. The canonical problems are solved using the filtering methods developed in [4], with spatial truncation $P_c = 50$. In cases other than head-on incidence, we have included results calculated using the $\{-\infty, \infty\}$ array solution (i.e. by replacing F_n^p with $e^{ikp \cos \psi_0} B_n$ in

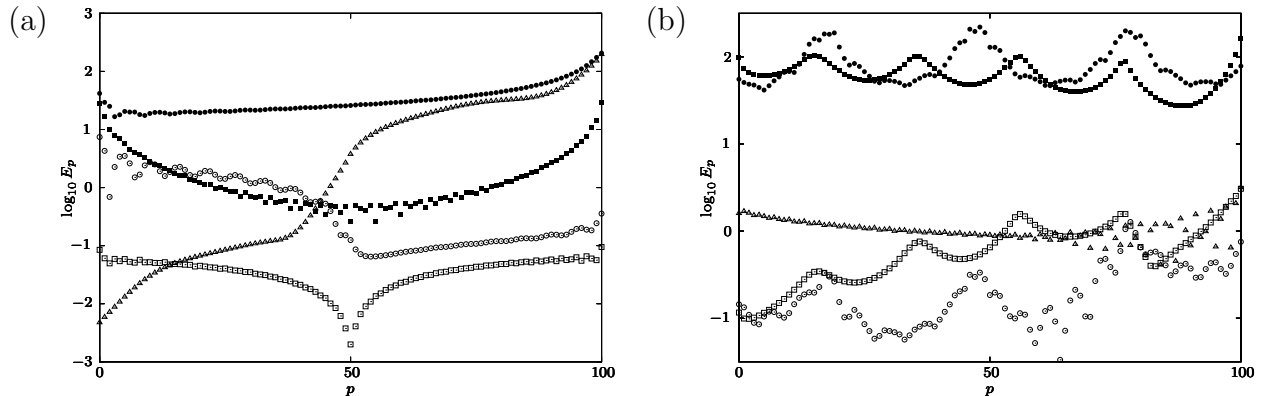


Figure 3: Percentage errors; shaded points are calculated using the $\{-\infty, \infty\}$ array, unshaded points use the large array approximation. (a) $\psi_0 = \pi/4$, $a = 0.25$, $k = 5.0$ (\square); $\psi_0 = \pi/4$, $a = 0.25$, $k \approx 3.68$ (\circ); $\psi_0 = 0$, $a = 0.25$, $k = 3.0$ (\triangle). (b) $\psi_0 = 0$, $a = 0.25$, $k = 2$ (\triangle); $\psi_0 = \pi/10$, $a = 0.25$, $k = 2.5$ (\circ); $\psi_0 = \pi/10$, $a = 0.49$, $k = 2.97$ (\square).

(38)) for comparison with those obtained via the large array approximation. In figure 3(a), square data points have been used to indicate percentage errors for $a = 0.25$, $k = 5.0$ and $\psi_0 = \pi/4$. Close to the centre of the array, the solution to the $\{-\infty, \infty\}$ problem exhibits an error around the 1% level, however this rises to around 10% near the ends. As there are no Rayleigh–Bloch waves in this case, the large array approximation improves on this by simply including decaying effects due to each end. The agreement is now very good, with the error falling to around 0.1% close to the ends, and lower elsewhere. It was noted in [12] that in a resonant case, the solution to the $\{-\infty, \infty\}$ problem bears less resemblance to the large finite array. This is now understood to be caused by the slower rate of decay exhibited by the end effects in such cases. Round data points have been used in figure 3(a) to indicate percentage errors for $a = 0.25$, and $\psi_0 = \pi/4$ with k chosen so as to create a left resonance with $j = -1$ in (9); thus $k \approx 3.681$. The errors in the $\{-\infty, \infty\}$ solution are indeed considerably larger than in the previous case, around 10% at best, rising to over 100% close to the right end. The large array approximation again offers a significant improvement, in particular for $p > 50$, where the errors are around 0.3%. There are two important points to note here. First, the errors are greater than in the previous case, because the large array approximation discards more significant effects in a resonant case. Secondly, the errors are greater on the left half of the array because for $p < 50$, \hat{C}_m^p must be calculated by approximating C_m^p in (22) via (37), with $u = 1/2$. Triangular points have been used to indicate errors for the case $a = 0.25$, $k = 3.0$, $\psi_0 = 0$. Since head-on incidence is a type of right-resonance, an increase in E_p occurs for $p > 50$. For $p < 50$, the errors are negligible, whereas for $p > 50$, the actual coefficients F_m^p are small, but the most significant effect is caused by the fact that the array does not extend to infinity on the right side, and this is neglected by the large array approximation. Consequently, the errors are relatively large.

Figure 3(b) shows some examples where Rayleigh–Bloch waves are present. The triangular data points correspond to the parameters $a = 0.25$, $k = 2.0$, $\psi_0 = 0$, for which symmetric Rayleigh–Bloch waves are present, and the error is seen to be around the 1% level. Round data points were computed using $a = 0.25$, $k = 2.5$ and $\psi_0 = \pi/10$. Symmetric Rayleigh–Bloch waves are again present, causing large errors to occur on all scatterers when

P	$T_{\text{ex}}(s)$	$(P_c = 50)$		$(P_c = 100)$	
		$T_{\text{la}}(s)$	$E_{\text{max}}(\%)$	$T_{\text{la}}(s)$	$E_{\text{max}}(\%)$
100	7.2	4.1	1.3	25.8	0.38
200	48.4	4.1	1.9	25.8	0.51
300	179.8	4.2	1.8	25.9	0.59

Table 2: Computation times (in seconds) and maximum percentage errors for various array sizes using $a = 0.25$, $k = 2.5$ and $\psi_0 = \pi/10$. Symmetric Rayleigh–Bloch waves are present in the solution.

the solution is approximated using the infinite array. This is corrected by the large array approximation, where the errors are now around 1%, at worst. Interestingly, the pattern of oscillations in E_p is similar to that which occurs in the infinite array solution, indicating that the remaining error is due to inaccuracies in computing the Rayleigh–Bloch wave amplitudes $\alpha(\psi_0)$ and $\alpha(\pi - \psi_0)$, and reflection coefficient ρ . Finally, square data points have been used to represent the case where $a = 0.49$, $k = 2.97$ and $\psi_0 = \pi/10$. Antisymmetric Rayleigh–Bloch modes now occur and large errors are evident when the infinite array solution is used. Again, these are corrected by the large array approximation where the error reaches around 3% at the right end, and is lower elsewhere.

The time required to construct the large array approximation is generally much shorter than that required to solve the $\{0, P\}$ array problem exactly. Table 2 shows computation times (using Fortran 2003 on a 2.5GHz Macintosh running OS X) with a typical set of parameters, for various array sizes. Symmetric Rayleigh–Bloch waves are present in the solution. The computation time for the exact solution, T_{ex} increases rapidly with the array size, P . In contrast, solving the canonical problems is the most expensive procedure required for the construction of the large array approximation; T_{la} is largely unaffected by the actual array size. The maximum percentage error, defined as

$$E_{\text{max}} = \max\{E_p : p \in \{0, P\}\}$$

is also shown. This is reduced by increasing P_c from 50 to 100, at the expense of increasing computation time. For $P_c = 50$, we have $E_{\text{max}} < 2\%$ for all of the array sizes shown; this is sufficiently accurate for many purposes.

4 Near-trapping

One of the motivations behind this present article is the association between trapped modes for cylinders in channels and large responses in the scattering by a long finite array in the open sea, first discovered by Maniar & Newman [5]. The trapped modes that they studied were for a single cylinder in a channel, but subsequently it was shown numerically [16, 17] (and later proved analytically [18]) that a number of different modes exist when the $\{0, P\}$ array (with $P > 0$) is situated in a channel with walls located at $x = -1/2$ and $x = P + 1/2$. For either Dirichlet or Neumann boundary conditions on the channel walls, the frequencies at which these modes can occur are given by

$$\tilde{\beta} = [1 - q/(P + 1)]\pi, \quad q \in \{0, 1, \dots, P\}; \quad (39)$$

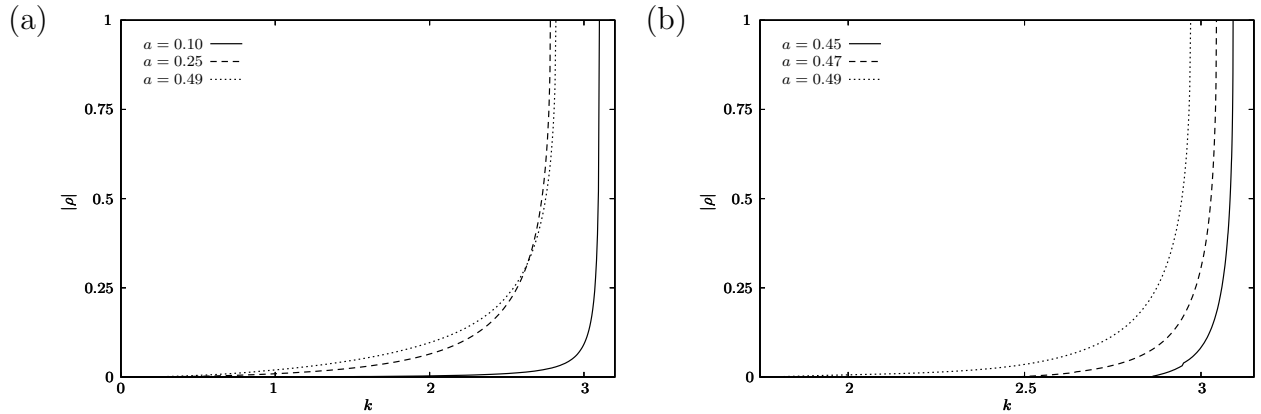


Figure 4: Modulus of the reflection coefficient ρ for (a) symmetric and (b) antisymmetric Rayleigh–Bloch waves.

this is an exact result. It has been noted that the frequencies at which large responses can occur in the problem of scattering by a long array in the open sea [7] are predicted by (39), with $0 < q \ll P + 1$. In this case it is an (albeit very accurate) approximation, as we shall see.

Now the large responses observed by Maniar & Newman in [5] do not occur in the case of scattering by an infinite or semi-infinite array. Furthermore, these effects have only been observed when the wavenumber k is such that Rayleigh–Bloch waves can exist. It therefore follows that a key role is played by interactions between the ends of the finite array, and in particular the reflection coefficient ρ . Figure 4 shows values of $|\rho|$ for different scatterer sizes and varying k , in both the symmetric and antisymmetric cases. In all cases, $|\rho|$ remains small, until k approaches k_{\max} , and then the magnitude increases sharply toward the limiting value $|\rho| = 1$. The fact that $|\rho| \rightarrow 1$ as $k \rightarrow k_{\max}$ shows that as the cut-off for Rayleigh–Bloch waves is approached the amount of energy scattered away from the array by reflections decreases. Coupled to this is the observation from [4] that $|\alpha|$ increases to its maximum value as $k \rightarrow k_{\max}$. Hence in the long finite array problem we should expect that large responses can only occur at or near $k = k_{\max}$.

In fact, taking $k = k_{\max}$ exactly (and therefore $\tilde{\beta} = \pi$) does not produce a large response. Although the denominator $1 - \rho\hat{\rho}$ in (35) vanishes in the limit $\tilde{\beta} \rightarrow \pi$, cancellation effects due to the standing wave nature of the Rayleigh–Bloch waves (see §2.2) cause their total contribution to (33) (i.e. $\chi^R \exp(ip\tilde{\beta})\tilde{B}_m \pm \chi^L \exp(-ip\tilde{\beta})(-1)^m\tilde{B}_m$) to remain finite. If k is slightly less than k_{\max} , so that $|\rho| \approx 1$, then we must consider the effect of interference between the left and right propagating Rayleigh–Bloch waves and their respective multiple reflections. Thus, a large response is expected to occur when the interference is purely constructive, and this corresponds to situations where the phase of the Rayleigh–Bloch wave is unchanged after traversing the array once in each direction, and so undergoing a single reflection by each end. That is, the quantity

$$\rho\hat{\rho} = \rho^2 e^{2iP\tilde{\beta}} \quad (40)$$

must be positive real. Given that $\rho = 1$ when $k = k_{\max}$ (see §2.2), an approximate formula for the values of $\tilde{\beta}$ near the cut-off at which pure constructive interference occurs is obtained by simply assuming that $\text{Im}[\rho] = 0$. However, in many cases of physical interest, including

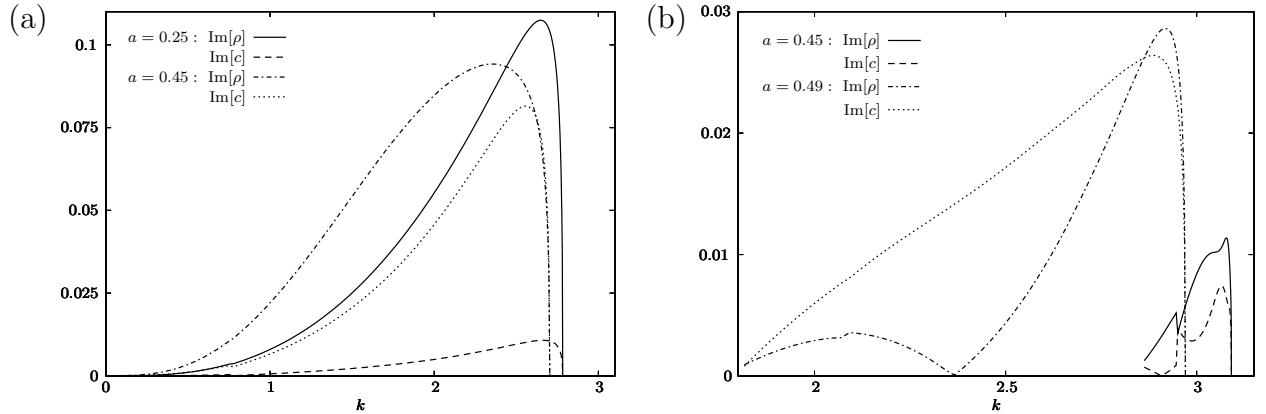


Figure 5: Imaginary parts of ρ and c for (a) symmetric and (b) antisymmetric Rayleigh–Bloch waves.

that investigated by Maniar & Newman ($a = 0.25$ in our notation), a better approximation is achieved by assuming that $\text{Im}[c] = 0$, where $c = \rho e^{-i\tilde{\beta}}$; in fact this yields precisely (39). That is, pure constructive interference occurs at or very close to those frequencies for which the Rayleigh–Bloch wave is $2(P + 1)$ periodic. Since $2(P + 1)$ periodicity of the Rayleigh–Bloch wave is a necessary and sufficient condition for the existence of a trapped mode in a channel containing the $\{0, P\}$ array, the connection between these phenomena and near-trapping on arrays in the open sea is now clear. However, we reiterate that $2(P + 1)$ periodicity is not a sufficient condition for near-trapping; we must also have $|\rho| \approx 1$, which in turn requires that $k \approx k_{\max}$. The imaginary parts of ρ and c for symmetric and antisymmetric Rayleigh–Bloch waves are shown in figure 5. The magnitude of the imaginary parts of both ρ and c are always relatively small, but for symmetric Rayleigh–Bloch waves on arrays of small scatterers, we have $|\text{Im}(c)| \ll |\text{Im}(\rho)|$ for k close to k_{\max} , the difference decreasing as the scatterer radius is increased. When $a = 0.45$ we have $|\text{Im}(c)| \approx |\text{Im}(\rho)|$ and for larger values $|\text{Im}(c)|$ can exceed $|\text{Im}(\rho)|$. Accurate values for antisymmetric waves are difficult to obtain. This is due to a combination of two factors. First, the size of the scatterers means that a large number of modes must be used in order to accurately represent the field. Secondly, the ratio of $\text{Re}[\rho]$ to $\text{Im}[\rho]$ is greater in this case, and, given that the filtering method in [4] can achieve only a limited number of significant figures, we should expect some numerical inaccuracies. Indeed, it is likely that these are responsible for the cusp in the curve for $a = 0.45$ in figure 5(b), despite the use of a large spatial truncation ($P_c = 300$) in generating the data. Nevertheless, it is evident from the figure that $|\text{Im}(c)| < |\text{Im}(\rho)|$ when k is close to k_{\max} , but the difference is small. Whatever approximation we use, i.e. $\text{Im}[c] = 0$ (which leads to (39)) or $\text{Im}[\rho] = 0$ (which leads to the same formula but with $P + 1$ replaced by P), it is clear that increasing P allows constructive interference to occur closer to the cut-off, and hence with an increased value for $|\rho|$. That is, near-trapping is enhanced on larger arrays.

One of the most significant effects of near-trapping is the possibility that large forces may be exerted on certain elements of the array, as in figure 1. Now the force exerted in the x and y directions on scatterer p , normalised using the force on a cylinder in isolation, are given by

$$\mathcal{F}_x^p = \frac{1}{2} |\mathcal{U}_1^p - \mathcal{U}_{-1}^p|, \quad \text{and} \quad \mathcal{F}_y^p = \frac{1}{2} |\mathcal{U}_1^p + \mathcal{U}_{-1}^p|, \quad (41)$$

respectively [10, §3]. Thus, as we should expect, $\mathcal{F}_x^p = 0$ for a field that is antisymmetric

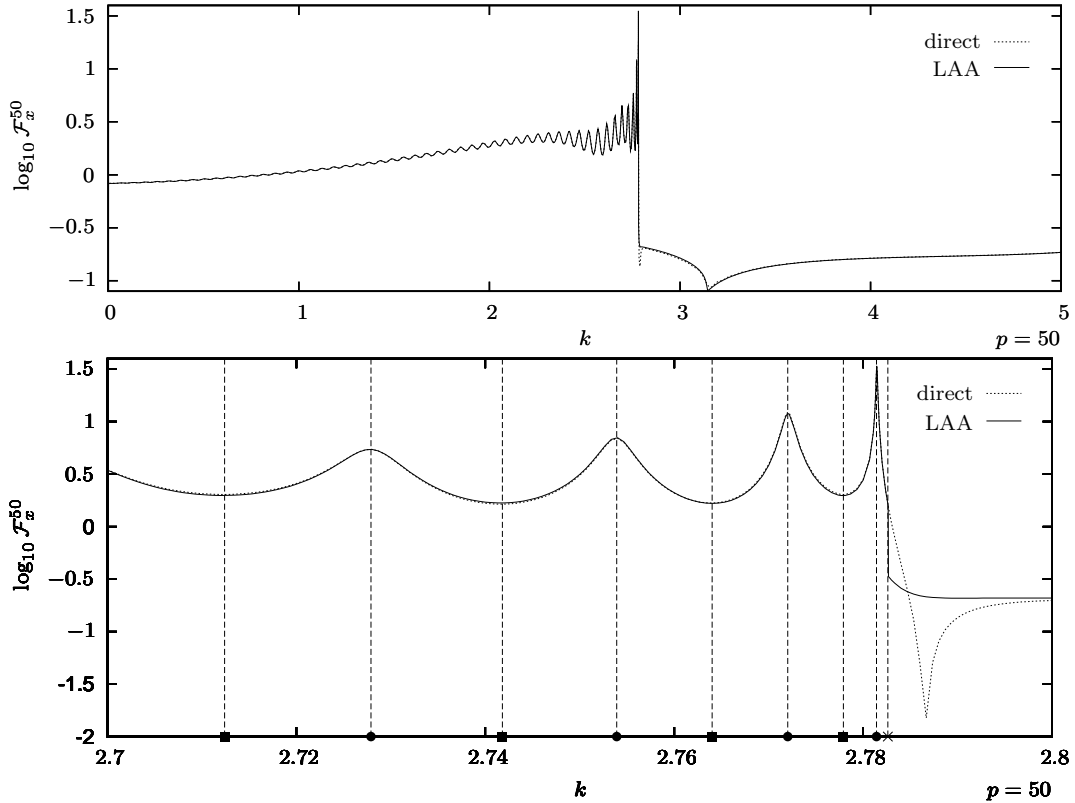


Figure 6: Force on cylinder 50 of a 101 scatterer array, at head-on incidence with $a = 0.25$ and varying k . Legend: \times cut-off for symmetric Rayleigh–Bloch modes, \bullet (\blacksquare): peak (minimum) predicted by (39) and (42). The dotted line is the full linear solution and the data for the solid line is obtained using the large array approximation. The lower plot is an expanded version of the upper plot near to $k = k_{\max}^s$.

about $y = 0$, whereas $\mathcal{F}_y^p = 0$ for a symmetric field (see equation (16)). It turns out that near-trapping of the symmetric Rayleigh–Bloch mode has the greater physical significance in this context. There are two reasons for this. First, as discussed in §2.2, for an antisymmetric wave $\tilde{B}_1 = \tilde{B}_{-1} \rightarrow 0$ as $k \rightarrow k_{\max}^a$. Furthermore, results in [4] show that the largest value for $\alpha(\psi_0)$ occurs at head-on incidence, when there is no antisymmetric field. In fact, the peak value of α is sufficiently large that the strongest near-trapping effects generally occur for $\psi_0 = 0$, despite the fact that $\alpha(\pi - \psi_0) = 0$ in this case.

Figure 6 shows logarithmic plots of the force on the center cylinder of a 101 scatterer array at head-on incidence, with $a = 0.25$ and varying k . The forces are calculated from (41) using either $\mathcal{U}_n^p = F_n^p$ for the large array approximation, or $\mathcal{U}_n^p = D_n^p$ where, as before D_n^p is the coefficient obtained when the $\{0, P\}$ array problem is solved directly. The accuracy achieved by the large array approximation is very good, except when k is slightly larger than the cut-off value k_{\max}^s . The cause of this is that $\tilde{\beta}$ moves off the real line as k increases beyond the cut-off. Thus, in place of the Rayleigh–Bloch wave there is now a mode which is evanescent in x , and this can still cause interactions between the ends when the imaginary part of $\tilde{\beta}$ is small. The locations at which at which peaks and troughs occur in the force plots can be predicted by the following considerations. From equations (33), (35) and (41), it can be seen that the forces due to the left- and right-propagating Rayleigh–Bloch waves

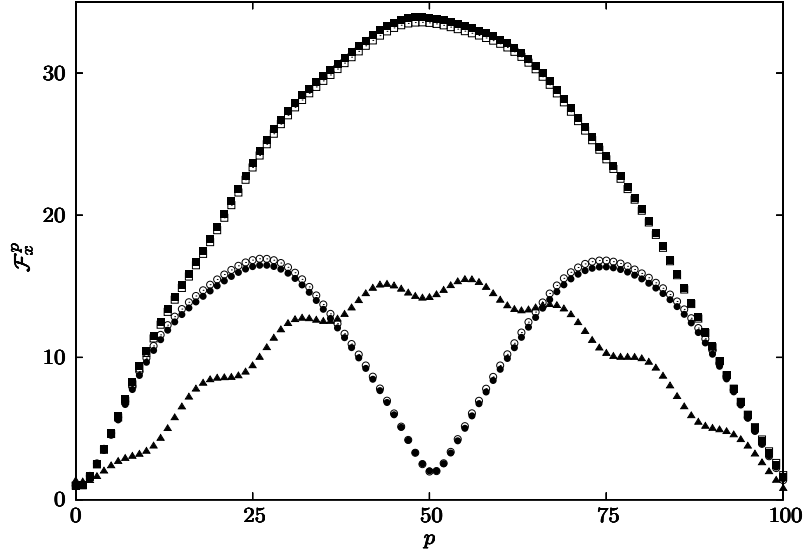


Figure 7: Normalised force on a 101 scatterer array, with $a = 0.25$. Shaded data points are exact results, unshaded use the large array approximation. $k \approx 2.7814$, $\psi_0 = 0$ (\square), $\psi_0 = \pi/10$ (\triangle); $k \approx 2.7778$, $\psi_0 = 0$ (\circ).

act in the same direction when the quantity $1 - \rho \exp(2i(P-p)\tilde{\beta})$ is maximised, whereas they act directly against each other when it is minimised. Retaining the assumption that, to a good approximation, $c = \rho e^{-i\tilde{\beta}}$ is negative real, and applying (39) (so as to achieve near-trapping), we find that

$$1 - \rho e^{2i(P-p)\tilde{\beta}} \approx 1 - |\rho| e^{iq\pi(2p+1)/(P+1)}. \quad (42)$$

If, as is the case here, we are concerned with the force at the centre of the array then, since $p = P/2$, odd and even values for q cause the forces to act in support of, and against each other, respectively. The corresponding frequencies are shown in figure 6 and the agreement is excellent.

Figure 7 shows the forces along the array, for fixed values of k . Shaded data points are obtained by solving the $\{0, 100\}$ problem directly; unshaded points use the large array approximation. The maxima and minima evident in the plots can be interpreted according to (42). Thus, data plotted with square points have been obtained by taking $\psi_0 = 0$, and setting $q = 1$ in equation (39), so that $k \approx 2.7814$ as in Maniar and Newman [5, figure 2b]. Here, equation (42) predicts that the forces due to the left and right Rayleigh–Bloch waves act in the same direction at centre of the array, and largely cancel each other at the ends. This behaviour is clearly evident in the plot. For comparison, data using the same parameters, but with $\psi_0 = \pi/10$ have been plotted using triangular data points. Here the agreement between the directly obtained solution and the large array approximation is such that the two sets of points are indistinguishable. The forces exhibit qualitatively similar behaviour to the head-on incident case, except that their magnitudes have been reduced, and the excitation of Rayleigh–Bloch waves by the incident field at the right end (which does not occur at head-on incidence) causes some interference. Similarly, the data plotted using circular points are also obtained at head-on incidence, but now setting $q = 2$ in equation (39), so that $k \approx 2.7779$. In this case, equation (42) predicts maximum forces at $p = 25$ and $p = 75$, and a minimum

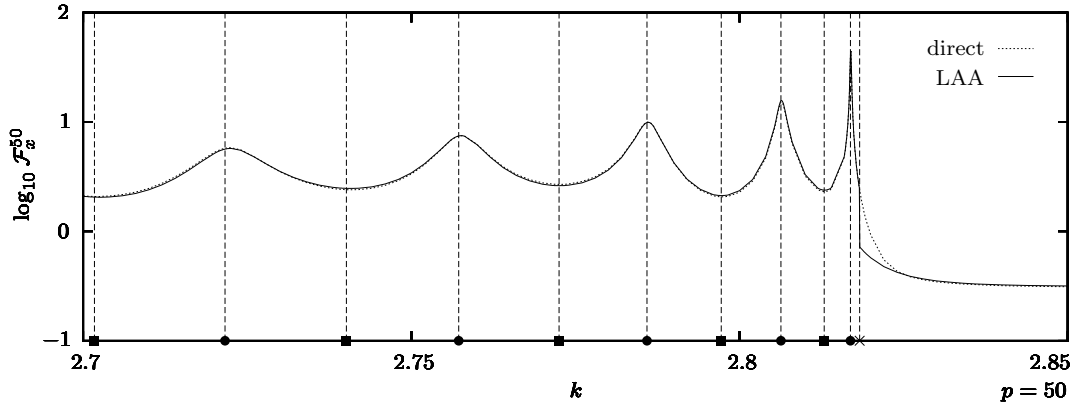


Figure 8: Force on cylinder 50 of a 101 scatterer array, at head-on incidence with $a = 0.49$ and varying k . Legend: \times cut-off for symmetric Rayleigh–Bloch modes, \bullet (\blacksquare): peak (minimum) predicted by (39) and (42). The dotted line is the full linear solution and the data for the solid line is obtained using the large array approximation.

at $p = 50$. Again, this behaviour is clearly evident in the plot.

As noted above, (39) is an approximation that is less good for larger scatterers. Figure 8 shows the horizontal force on cylinder 50 of a 101 scatterer array, with $a = 0.49$ at head-on incidence with varying k . As before, the agreement between the large array approximation and the exact theory is excellent, except for a small discrepancy which occurs when k is slightly greater than k_{\max}^s , so that the Rayleigh–Bloch wave is replaced by a mode that is weakly evanescent in x . The predictions made by (39) for the frequencies at which maximum and minimum forces occur are less accurate than for $a = 0.25$, though the errors are small.

5 Conclusion

We have shown in this article how the response of a long finite array to an incident plane wave can be modelled accurately and efficiently by decomposing it into a set of canonical problems formulated on infinite and semi-infinite arrays. This can lead to considerable computational savings. Moreover, the decomposition provides a powerful explanation of the near-trapping phenomenon that has been observed for this type of array. We have formulated the problem as a water-wave scattering problem involving an array of vertical circular cylinders, but exactly the same mathematical problem arises in certain applications in acoustics, electromagnetism and elasticity involving circular scatterers. The same theory can be applied to arrays made up of more general shapes of scatterer, provided the canonical problems for these scatterers can be solved.

Acknowledgements

IT is supported by EPSRC under grant EP/C510941/1.

References

- [1] Mohammad R. Zunoubi and Hassan A. Kalthor. Diffraction of electromagnetic waves by periodic arrays of rectangular cylinders. *J. Opt. Soc. Am., A*, 23:306–313, 2006.
- [2] D. S. Janning and B. A. Munk. Effects of surface waves on the currents of truncated periodic arrays. *IEEE Trans. Antennas Propagat.*, 50(9):1254–1265, 2002.
- [3] D. R. Jackson, J. T. Williams, A. K. Bhattacharyya, R. L. Smith, S. J. Buchheit, and S. A. Long. Microstrip patch designs that do not excite surface waves. *IEEE Trans. Antennas Propagat.*, 41(8):1026–1037, 1993.
- [4] C. M. Linton, R. Porter, and I. Thompson. Scattering by a semi-infinite periodic array and the excitation of surface waves. *SIAM J. Appl. Math.*, 67(5):1233–1258, 2007.
- [5] H. D. Maniar and J. N. Newman. Wave diffraction by a long array of cylinders. *J. Fluid Mech.*, 339:309–330, 1997.
- [6] P. McIver, C. M. Linton, and M. McIver. Construction of trapped modes for wave guides and diffraction gratings. *Proc. Roy. Soc. Lond., A*, 454:2593–2616, 1998.
- [7] D. V. Evans and R. Porter. Trapping and near-trapping by arrays of cylinders in waves. *J. Engng. Math.*, 35:149–179, 1999.
- [8] S. V. Sukhinin. The whispering surface effect. *J. Appl. Maths Mechs*, 63(6):863–876, 1999.
- [9] C. M. Linton and M. McIver. The existence of Rayleigh-Bloch surface waves. *J. Fluid Mech.*, 470:85–90, 2002.
- [10] C. M. Linton and D. V. Evans. The interaction of waves with arrays of vertical circular cylinders. *J. Fluid Mech.*, 215:549–569, 1990.
- [11] C. M. Linton and D. V. Evans. The interaction of waves with a row of circular cylinders. *J. Fluid Mech.*, 251:687–708, 1993.
- [12] C. M. Linton and I. Thompson. Resonant effects in scattering by periodic arrays. *Wave Motion*, 44:167–175, 2007.
- [13] V. Twersky. Elementary function representation of Schlömilch series. *Arch. Rational Mech. Anal.*, 8:323–332, 1961.
- [14] C. M. Linton. Schlömilch series that arise in diffraction theory and their efficient computation. *J. Phys. A*, 39:3325–3339, 2006.
- [15] C. M. Linton and P. A. Martin. Semi-infinite arrays of isotropic point scatterers. A unified approach. *SIAM J. Appl. Math.*, 64(3):1035–1056, 2004.
- [16] T. Utsunomiya and R. Eatock Taylor. Trapped modes around a row of circular cylinders in a channel. *J. Fluid Mech.*, 386:259–279, 1999.
- [17] R. Porter and D. V. Evans. Rayleigh-Bloch surface waves along periodic gratings and their connection with trapped modes in waveguides. *J. Fluid Mech.*, 386:233–258, 1999.
- [18] C.M. Linton and M. McIver. Periodic structures in waveguides. *Proc. Roy. Soc. Lond., A*, 458:3003–3021, 2002.